

Article

# Mineralogical Transformations of Heated Serpentine and Their Impact on Dissolution during Aqueous-Phase Mineral Carbonation Reaction in Flue Gas Conditions

Clémence Du Breuil <sup>1</sup>, Louis César-Pasquier <sup>1,\*</sup> , Gregory Dipple <sup>2</sup>, Jean-François Blais <sup>1</sup>, Maria Cornelia Iliuta <sup>3</sup> and Guy Mercier <sup>1</sup>

<sup>1</sup> Institut National de la Recherche Scientifique (Centre Eau, Terre et Environnement), University of Quebec, 490 rue de la Couronne, Quebec, QC G1K 9A9, Canada; clemence.jouveau\_du\_breuil@inrs.ca (C.D.B.); jean-francois.blais@ete.inrs.ca (J.-F.B.); guy.mercier@ete.inrs.ca (G.M.)

<sup>2</sup> Department of Earth, Ocean and Atmospheric Sciences, University of British Columbia, 2020–2207 Main Mall, Vancouver, BC V6T 1Z4, Canada; gdipple@eoas.ubc.ca

<sup>3</sup> Chemical Engineering Department, Laval University, Quebec, QC G1V 0A6, Canada; maria-cornelia.iliuta@gch.ulaval.ca

\* Correspondence: louis-cesar.pasquier@ete.inrs.ca; Tel.: +1-418-654-2606; Fax: +1-418-654-2633

Received: 16 August 2019; Accepted: 23 October 2019; Published: 3 November 2019



**Abstract:** Mineral carbonation is known to be among the most efficient ways to reduce the anthropogenic emissions of carbon dioxide. Serpentine minerals ( $Mg_3Si_2O_5(OH)_4$ ), have shown great potential for carbonation. A way to improve yield is to thermally activate serpentine minerals prior to the carbonation reaction. This step is of great importance as it controls  $Mg^{2+}$  leaching, one of the carbonation reaction limiting factors. Previous studies have focused on the optimization of the thermal activation by determining the ideal activation temperature. However, to date, none of these studies have considered the impacts of the thermal activation on the efficiency of the aqueous-phase mineral carbonation at ambient temperature and moderate pressure in flue gas conditions. Several residence times and temperatures of activation have been tested to evaluate their impact on serpentine dissolution in conditions similar to mineral carbonation. The mineralogical composition of the treated solids has been studied using X-ray diffraction coupled with a quantification using the Rietveld refinement method. A novel approach in order to quantify the meta-serpentine formed during dehydroxylation is introduced. The most suitable mineral assemblage for carbonation is found to be a mixture of the different amorphous phases identified. This study highlights the importance of the mineralogical assemblage obtained during the dehydroxylation process and its impact on the magnesium availability during dissolution in the carbonation reaction.

**Keywords:** serpentinite; X-ray diffraction; rietveld refinement; magnesium leaching; thermal activation; meta-serpentine; carbonation; heat activation optimization

## 1. Introduction

The increasing greenhouse gas emissions and particularly anthropogenic carbon dioxide ( $CO_2$ ) in the atmosphere are known to play a major role in climate change [1]. Mitigation solutions are needed more than ever. Among the methodologies proposed for mitigation, mineral carbonation appears to be one of the most sustainable [2,3]. This natural and spontaneous phenomenon involves the reaction between  $CO_2$  (aqueous or gas) and divalent cations bearing minerals in order to form the associate carbonates [3]:

Equation (1) Carbonation reaction [4]

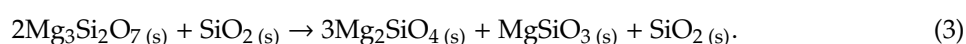
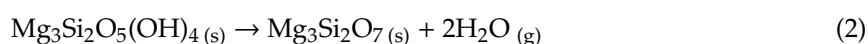


The reaction products are stable and inert solids where  $\text{CO}_2$  is sequestered. The composition of the resulting carbonates depends on the major cations present in the reactant mineral [5]. Carbonation reaction can be divided in three main steps: (i) the  $\text{CO}_2$  dissolution in water (ii) the material dissolution and (iii) the precipitation of carbonates as final products. The process is essentially controlled by the first two steps [6]. Serpentine minerals, due to their high amount of  $\text{Mg}^{2+}$  [7] are considered for carbonation [8]. Thermal treatment acts on serpentine dissolution by enhancing  $\text{Mg}^{2+}$  availability, making it a key step for the process [9]. Serpentine dissolution first results in a rapid exchange of surfacing  $\text{Mg}^{2+}$  with protons ( $\text{H}^+$ ) before being extracted from the structure into the solution, during a much slower phase [10,11]. The dissociation of  $\text{CO}_2$  added to the solution will generate protons and  $\text{HCO}_3^-$  ions, therefore enhancing  $\text{Mg}^{2+}$  availability (Pasquier et al., 2014b).

Lizardite, antigorite, and chrysotile are the main minerals of the serpentine group ( $\text{Mg}_3\text{Si}_2\text{O}_5(\text{OH})_4$ ), belonging to the phyllosilicate class [7,12–14]. Serpentine structure is made of stacked layers composed of two sheets: the tetrahedral layer composed of silicon tetrahedral ( $\text{SiO}_4$ ), linked to the lateral Mg of the octahedral layer by its apical oxygen atoms, forming a covalent bond [14,15]. Outer hydroxyl groups contribute to Van der Waals interactions between the two layers, whereas inner hydroxyl groups contribute to intrafoliar Van der Waals interactions [15–17].

Under high temperatures, hydroxyl groups, linked to Mg atoms, escape the structure. During this dehydroxylation process, serpentine transformed into amorphous phases (between 550 and 750 °C—Equation (2)), and then recrystallized into forsterite ( $\text{Mg}_2\text{SiO}_4$  > 750 °C), associated with enstatite ( $\text{MgSiO}_3$  > 800 °C) as the temperature increased (Equation (3)) [18–20]. Two types of amorphous phases have been described [21]: pseudo-amorphous phases, named  $\alpha$ -meta-serpentine, appearing at 50% of the total dehydroxylation reaction, and amorphous meta-serpentine, appearing at 90% of the total dehydroxylation. The formation of  $\alpha$ meta-serpentine component can be observed at a temperature close to 580 °C visualized on a diffractogram by a feature in the lower angle domain ( $2\theta = \pm 6^\circ$ ) [21].

Equations (2) and (3): Serpentine dihydroxylation



It has been observed that amorphous meta serpentine tends to promote  $\text{Mg}^{2+}$  leaching and thus carbonation [21–23]. Therefore, optimized conditions for carbonations have been prescribed to be between 630 °C and 650 °C for 30 to 120 min [22,24,25]. However, in the previous studies, carbonation reactions have essentially been performed using pure  $\text{CO}_2$  gas at high temperature and high pressure [21,25–27], strong acids or salts to promote dissolution [22,28]. To date no studies have been conducted on optimizing thermal activation from the mineralogical point of view, especially for direct aqueous mineral carbonation using diluted gas. In these conditions, serpentine dissolution is only promoted by carbonic acid at room temperature and low/mild  $\text{CO}_2$  partial pressure and a good activation is more than ever critical for reaction.

This study is part of the follow-up work on direct flue gas carbonation process initiated by Mercier et al. at INRS, Québec [29]. Using mining residues available in the Province of Québec, the process uses a simulated cement plant flue gas to perform direct flue gas aqueous carbonation [30]. Carbonation reaction parameters have been optimized by Pasquier [31], optimized conditions for the precipitation of carbonates have been determined by Moreno [32] whereas a technical and economical evaluation of the process have shown its feasibility and sustainability in the Province of Québec [33]. However, a pilot scale test revealed that thermal treatment conditions needed to be optimized for the INRS process as well [34,35].

In the present paper, only the proportion of magnesium prior to precipitation will be studied and considered as an intermediate product of the carbonation, as thermal activation can only acts on enhancing serpentine dissolution. Therefore, post-carbonation solids were not considered in the present study for the given reasons. Furthermore, it serves to give a novel approach of evaluating the influence of amorphous phases on serpentine dissolution and thus  $Mg^{2+}$  leaching during direct flue gas aqueous mineral carbonation by introducing a new quantifying method of those phases. Those new mineralogical data will provide a further understanding of the relation between thermal activation and serpentine dissolution and therefore, improve this step in the INRS carbonation process.

## 2. Materials and Methods

### 2.1. Sample Preparation, Characterization and Analytical Methods

Serpentinite residues were sampled on stockpiles from Jeffrey Mine, near the town of Asbestos, southern of the Province of Québec. Lizardite is identified to be the major serpentine polymorph [36]. Fibres, representing 20 wt % of the residue, were removed by gravimetric separation based on their buoyancy. Iron oxides were also removed by wet gravimetric separation using the Wifley table, due to their potential commercial value for the process.

The sample was ground using a ring mill (Retsch RS200, Dusseldorf, Germany). The grain size distribution is given in Table 1. Values were obtained and measured using a particle size distribution analyzer (LA-950V2 Horiba, Kyoto, Japan).

**Table 1.** Size distribution of the sample.

Mean Size ( $\mu\text{m}$ )	$d_{90}$	$d_{50}$	$d_{10}$
16.00	1.99	8.16	43.28

The chemical composition of the starting material is given in Table 2. The chemical composition of liquid and solid samples was obtained using inductively coupled plasma-atomic emission spectrometry (ICP-AES) analysis (Varian, Palo Alto, CA, USA). Solid samples were first fused using the Claisse Method [37]. Loss on ignition (LOI) was obtained from mass difference after placing the sample into a ceramic crucible inside a muffle furnace for 6 h at 1025 °C.

**Table 2.** Composition of the raw solid feedstock <sup>1</sup>.

Elements	Values (wt %)
CaO	0.7
Cr <sub>2</sub> O <sub>3</sub>	0.2
Fe <sub>2</sub> O <sub>3</sub>	6.8
K <sub>2</sub> O	0.2
MgO	41.0
MnO	0.1
NiO	0.3
SiO <sub>2</sub>	39.9
LOI	10.8

<sup>1</sup> Major compounds only.

Phases were identified using XRPD analysis (Bruker AXS, 2004, Karlsruhe, Germany), performed at the University of British Columbia. To prepare the sample, 1.6 g were mixed with 0.4 g of pure corundum (Al<sub>2</sub>O<sub>3</sub>) [38], used as an internal standard, representing a 20.0 wt % spike. Samples were ground in ethanol using agate grinding pellets for seven minutes, in a McCrone micronizing mill to ensure homogenization. Scans were acquired for 30 min with  $2\theta$  ranging from 3° to 80° with scanning step size of  $2\theta = 0.3^\circ$  with a counting time of 7 s per step, on a Siemens D5000 Bragg-Brentano  $\theta$ - $2\theta$

diffractometer (Bruker AXS, 2004, Karlsruhe, Germany) with radiation  $\text{CuK}\alpha$  (40kV, 40mA). Matches were obtained using Bruker identification software DIFFRACplus EVA and the ICDD PDF-2 database.

Quantification of phases was performed using the Rietveld method ([39–42]) based on a calibration factor obtained from the mass and volume of each phase's unit cell. However, this method requires that all of the phases show high degrees of crystallinity with well-defined crystal structures [42]. Serpentine minerals are known to show discrepancies from their ideal crystal structures [38,43]. Therefore, when the crystalline structure of a phase is unknown or partially known, it can be quantified through the use of the Partial Or No Known Crystalline Structure method (PONKCS), combined with the Rietveld method [44]. A standard sample of pure chrysotile (90.0 wt %) and fluorite (10.0 wt %), provided by The University of British Columbia (Vancouver, British Columbia, Canada), whose composition is well known [38] was used in order to calibrate the PONKCS model. A calibrated mass value for the unit cell of both phases was acquired by Rietveld refinements and the chrysotile peaks were fitted using the Le Bail method [45]. The unit cell parameters and the space group were extracted from Falini [46]. The generated PONKCS model was then used in the Rietveld refinements as a crystallographic information files in the software TOPAS (Bruker AXS) [44,47].

## 2.2. Experimental Apparatus and Conditions

### 2.2.1. Thermal Activation

Heat treatments were performed in a muffle furnace, Furnatrol I33 (Thermolyne Subron Corporation). Twenty grams of samples were placed in a cast-iron skillet in a thin surface, then introduced into the furnace. Cast iron was chosen for its resistance to drastic temperature changes. No major iron contaminations were observed after thermal treatments according to chemical analysis. Tests were performed under isothermal conditions, meaning that the furnace was set to the targeted temperature beforehand to the test. At the end of the treatment, the furnace was open to help the skillet cool down, for five minutes. The skillet and the sample were weighted and the difference between initial and final masses corresponded to the mass lost induced by heat treatment. A series of seven tests were conducted at different residence times and temperatures, as shown in Table 3.

**Table 3.** Treatment conditions.

Residence Time (min)	Temperature (°C)		
	550	650	750
15	A	C	F
30	-	D	G
60	B	E	H

### 2.2.2. Dissolution in Aqueous Carbonation Conditions

Dissolution reactions were performed using carbonation conditions in order to evaluate thermal treatment effects on the developing process. Carbonation reactions were conducted in a 300 mL stirred reactor, model 4561 of Parr Instrument Company (Moline, IL, USA) [29,31]). The tests were performed using a certified composition gas of 4.0 vol%  $\text{O}_2$  and 18.2 vol%  $\text{CO}_2$ , balanced with  $\text{N}_2$ , simulating cement plant flue gas. The pulp density was set to 15% ( $150 \text{ g}\cdot\text{L}^{-1}$ ), with a volume of 75 mL of water, 11.25 g of solid and a gas phase volume of 225 mL, as optimized by Mercier et al. [29]. A batch of 10.2 bar of gas was introduced into the stirred reactor and was allowed to react with the pulp for 15 min at room temperature  $22 \text{ }^\circ\text{C} \pm 3 \text{ }^\circ\text{C}$  with the agitation sets to 600 RPM (Figure 1). As the reaction happens, the pressure decreased between 0.1 and 3.5 bar, depending on the amount of gas initially introduced. At the end of each batch, the pulp was filtered to obtain the liquid for chemical composition analyses. The reactivity of the eight thermally treated samples were tested along with an untreated sample (U). They were only observed throughout the proportion of magnesium leached from the solid during the reaction, using Equation (4)  $[\text{Mg}]_{\text{liq}}$  corresponds to the measured concentration of  $\text{Mg}^{2+}$  at the end of

the reaction,  $V$  and  $m$  are the volume of the solution and the mass of solid, respectively, and  $C_{Mg}$  is the measured concentration of Mg in the post-thermal treatment solid. Carbonates were not precipitated from the solution as thermal activation impacts on the Mg leaching. Mg analysis was performed on liquid sample after reaction. The liquid fraction was obtained after filtration of the resulting pulp. Consistency in the procedure was validated by performing mass balance to highlight any precipitation occurring during manipulation or during the pressure release of the vessel.

Equation (4): Proportion of  $Mg^{2+}$  leached

$$\%Mg = \frac{([Mg]_{liq} \times V) \times 100}{(C_{Mg} \times m)}. \quad (4)$$

In a successive batches test, the solid was used for 12 batches of gas. Every two batches, the solid was filtered and reused with fresh liquid in the subsequent batches. After six batches, the solid was filtered, dried at 60 °C, and ground for 1 min at 700 RPM in a ring mill, to partially remove the silica layer formed around the grains and then re used for another series of 6 batches as described by Figure 2. The liquid phase was sampled and renewed every two batches to prevent saturation. Long term reactivity of samples D and F treated at 650 °C for 30 min and 750 °C for 15 min, respectively, were tested in a successive batches experiment.

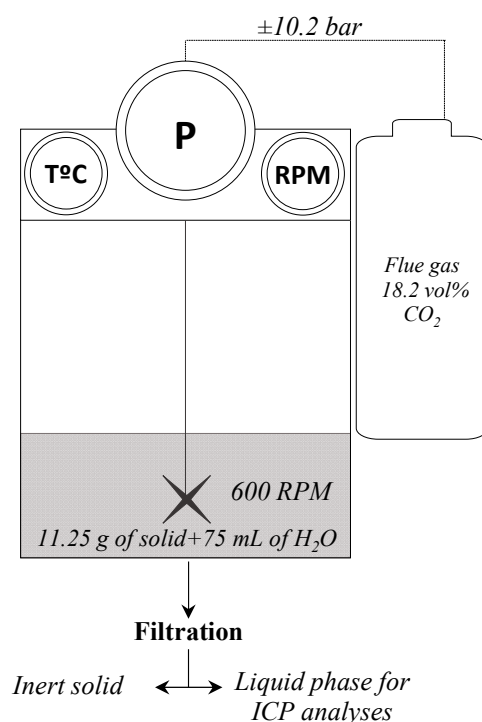


**Figure 1.** Parr reactor experimental set up.

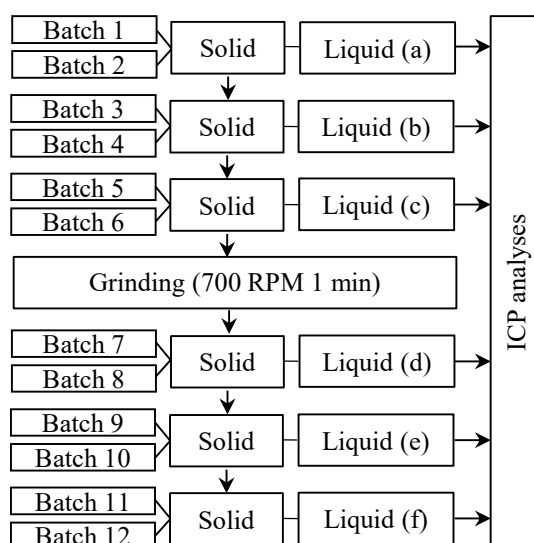


**Figure 2.** Batches dissolution experiments.

### 3. Results and Discussion

#### 3.1. Mass Loss

The proportion of mass lost by each sample during thermal treatments has been registered and is presented in Table 4. As expected, the proportion of mass lost during treatment increased with the temperature. It reached a peak at 14.5% for sample F and was treated at 750 °C for 15 min. This value is in agreement with the expected one, between 12.0% and 14.0% [48,49].

**Table 4.** Mass lost during each thermal treatment, expressed as percent of initial mass of sample.

Temperature (°C)	550		650			750			LOI
Residence Time (min)	15	60	15	30	60	15	30	60	
Sample Name	A	B	C	D	E	F	G	H	
% Mass Lost	5.5	5.5	5.0	9.9	12.5	14.2	13.1	11.7	10.8

#### 3.2. Mineralogical Transformations Along with Activation Temperatures

The evolution in the mineral composition at different temperatures and residence times has been studied using XRPD. Serpentine shows high crystallinity in samples U, A, and B, respectively untreated, treated at 550 °C for 15 min, and treated for 60 min. It then decreases in samples C, D, E, and F, respectively treated at 650 °C for 15 min, 30 min, and 60 min, and at 750 °C for 15 min. Crystalline features disappear in samples F and G, respectively, at 750 °C for 15 and 30 min. Amorphous contents can be identified in all of the treated samples as the crystallinity decreases. Forsterite is observed in samples E, G, and H, shown by highly crystalline peaks.

The remaining magnetite (the small proportion not removed during gravimetric separation) shows peaks in all samples, whereas the hematite (Fe<sub>2</sub>O<sub>3</sub>) which appears during the duration and temperature of the test increases. Due to the tests being performed in atmospheric conditions, the iron in the ferrous form (Fe<sup>2+</sup>) contained in the serpentine structure is oxidized into ferric iron (Fe<sup>3+</sup>) [50]. As iron rich olivine (fayalite—Fe<sub>2</sub>SiO<sub>4</sub>) can essentially incorporate Fe<sup>2+</sup> in its structure [51], hematite (Fe<sub>2</sub>O<sub>3</sub>) is preferentially formed.

Table 5 presents phases quantification as measured using the Rietveld refinement. Three issues are faced: (i) these values do not consider the mass loss occurring during thermal treatment (ii) amorphous components are identified in the untreated sample, due to the stacking disorder of serpentine, making

the identification of thermally induced amorphous components difficult, and finally (iii) a small peak is observed in the low angle that can be attributed to illite thus undermining the observation of the formation of meta-serpentine as described by [21]. Wilson et al. [38] determine that absolute quantification errors (wt %) for serpentine (chrysotile) and non-serpentine phases, regardless of their abundance in a sample, to be under 5.0 wt %. Consequently, illite is not considered in the Rietveld refinement as their peaks are too low and would fall under the estimation limit.

**Table 5.** Mineral composition using Rietveld refinements on XRD patterns, given in wt %.

		Amorphous	Serpentine	Forsterite	Magnetite	Hematite
Untreated	U	39.6	55.8	0.0	4.4	0.0
550 °C	A (15 min)	40.4	54.9	0.0	4.1	0.4
	B (60 min)	39.2	56.3	0.0	3.5	0.8
650 °C	C (15 min)	44.5	50.8	0.0	3.6	0.9
	D (30 min)	43.5	51.6	0.0	3.4	1.3
	E (60 min)	46.9	46.3	2.4	2.4	1.8
750 °C	F (15 min)	70.1	19.8	0.0	6.0	4.1
	G (30 min)	67.9	0.0	28.5	0.0	3.6
	H (60 min)	61.8	0.0	34.6	0.0	3.7

In an attempt to overcome these issues, a mass factor (MF in Equation (5)) is computed based on the mass loss of each sample (Table 4). Using this factor, the abundance of each phase can be expressed as grams per 100 g of starting material as given in Equation (5).

Equation (5): Proportion of phases expressed in mass

$$m_{\text{phase}} = \% \text{phase} \times \left( \frac{100}{100 + \% \text{mass loss}} \right) = \% \text{phase} \times \text{MF}. \quad (5)$$

As dehydroxylation is considered to be the loss of H<sub>2</sub>O from the structure, the mass of H<sub>2</sub>O lost per gram of serpentine is computed in order to obtain the proportion of dehydroxylated serpentine (Equation (6)). The value used as maximum mass loss “%mass loss<sup>max</sup>” was obtained experimentally and found to be 14.2% for this material.

Equation (6): Proportion of dehydroxylated serpentine

$$\% \text{ dehydroxylated serpentine} = \frac{\% \text{mass loss} / \sum (m_{\text{amorphous}} + m_{\text{serpentine}})}{\% \text{mass loss}^{\text{max}}} = \frac{m_{\text{H}_2\text{O lost}}}{\% \text{mass loss}^{\text{max}}}. \quad (6)$$

The initial remaining material is decomposed into a non-reacted serpentine (serpentine<sub>(i)</sub>) associated with a non-reacted amorphous phase (amorphous<sub>(i)</sub>) induced by the layered structure of the serpentine. Their masses are calculated according to Equation (7), assuming that amorphous phase and crystalline initial serpentine both dehydroxylated in the same proportion.

Equation (7): Mass of initial phases

$$m_{\text{phase}(i)} = (m_{\text{phase}}) - (m_{\text{phase}} \times \% \text{ dehydroxylated serpentine}). \quad (7)$$

The amount of dehydroxylated serpentine and amorphous phase corresponding to the first amorphous observed, (respectively named serpentine<sub>(d)</sub> and amorphous<sub>(d)</sub>) are given by Equation (8).

Equation (8): Mass of intermediate amorphous phases

$$m_{\text{phase}(d)} = m_{\text{phase}} - m_{\text{phase}(i)}. \quad (8)$$

Further dehydroxylation leads to the formation of meta-serpentine, whose mass is obtained by Equation (9). This formation is marked by the total loss of the hydroxyl groups at close to 10 wt % of the starting material mass.

Equation (9): Mass of meta-serpentine

$$m_{\text{meta-serpentine}} = (m_{\text{amorphous}} \times m_{\text{H}_2\text{O lost}}) - m_{\text{amorphous}_{(i)}} \quad (9)$$

As a result, three phases emerge from this calculation: first an initial serpentine, resulting from the sum of  $\text{amorphous}_{(i)}$  and  $\text{serpentine}_{(i)}$ , then an intermediate amorphous components which is the sum of  $\text{amorphous}_{(d)}$  and  $\text{serpentine}_{(d)}$  corresponding to the first stage of amorphization, and finally meta-serpentine. Forsterite and iron oxides (magnetite and hematite) remain unaltered by the calculation.

As shown in Table 6, Serpentine is gradually replaced by intermediate amorphous phases in samples treated at temperatures lower than 650 °C and peaks for 60 min treatment at 70.3 g/100 g of starting material. Meta-serpentine is first found in samples treated at 650 °C for 15 min. Its proportion increases with the temperature and peaks at 27.2 g/100 g of starting material in the sample treated at 750 °C for 15 min. The increase of meta-serpentine is combined with a decrease of intermediate amorphous components contents. As seen previously (Table 5), forsterite is observed in samples E, G and H, respectively treated at 650 °C for 60 min and at 750 °C for 30 and 60 min. A treatment at 750 °C for 15 min produced a sample with no initial serpentine and no forsterite but only amorphous phases, associated with iron oxides. These observations are in agreement with previous studies which observed the formation of an intermediate amorphous component,  $\alpha$  meta-serpentine, progressively replacing serpentine below 580 °C. It is then followed by the appearance of an amorphous meta-serpentine material by 650 °C prevailing by 750 °C [21].

**Table 6.** Mineralogical compositions based on Rietveld refinements, expressed in grams per 100 g of starting material) at given temperature and residence times. In. Serp: Initial serpentine, Inter. Am.: Intermediate amorphous components, Meta-serp.: Meta-serpentine, For.: forsterite, Mag: magnetite, Hem: hematite and ML: Mass loss.

		In. Serp.	Inter. Am.	Meta-Serp.	For.	Mag.	Hem.	ML
<b>Untreated</b>	<b>U</b>	95.6	0.0	0.0	0.0	4.4	0.0	0.0
<b>550 °C</b>	A (15 min)	52.8	36.5	0.0	0.0	3.9	0.4	5.5
	B (60 min)	53.5	37.0	0.0	0.0	3.3	0.8	5.5
<b>650 °C</b>	C (15 min)	54.0	31.9	4.8	0.0	3.4	0.9	5.0
	D (30 min)	21.6	60.3	4.0	0.0	3.0	1.2	9.8
	E (60 min)	4.2	70.3	7.2	2.1	2.1	1.6	12.5
<b>750 °C</b>	F (15 min)	0.0	49.9	27.2	0.0	5.2	3.5	14.2
	G (30 min)	0.0	33.6	25.5	24.8	0.0	3.1	13.1
	H (60 min)	0.0	34.3	20.3	30.5	0.0	3.2	11.7

### 3.3. Impact of Mineralogy on Dissolution

#### 3.3.1. Two Batches Dissolution

It is known that the amount of  $\text{Mg}^{2+}$  available for leaching will directly control, along with the amount of  $\text{CO}_2$  treated, the quantity of carbonates being precipitated from the liquid phase after carbonation [30,31]. This study focuses on the proportion of  $\text{Mg}^{2+}$  leached from thermally treated serpentine samples. Figure 3 shows the mass of intermediate amorphous components and of meta-serpentine added up and plotted against the proportion of  $\text{Mg}^{2+}$  leached into the liquid phase during the carbonation reaction. As the amount of amorphous components increases from none (U—untreated sample) to 77 g/ 100 g of starting material (F—750 °C 15 min), the proportion of  $\text{Mg}^{2+}$

leached during two batches of gas increases too, respectively from 3.3 wt % to 13.5 wt % of initial  $Mg^{2+}$  concentration in solid. Samples D, G and H show similar proportions of  $Mg^{2+}$  leached and a close amount of amorphous components. However, initial serpentine constitutes a third of the former composition, whereas forsterite is formed in the two latter. As observed in previous studies at 650 °C, the solubility of  $Mg^{2+}$  ions is first increased by thermal treatment until it is reduced with the decreasing content of amorphous phases and the formation of forsterite. The amount of  $Mg^{2+}$  leached from the heat activated serpentine appears to be linearly dependent on the proportion of amorphous phases.

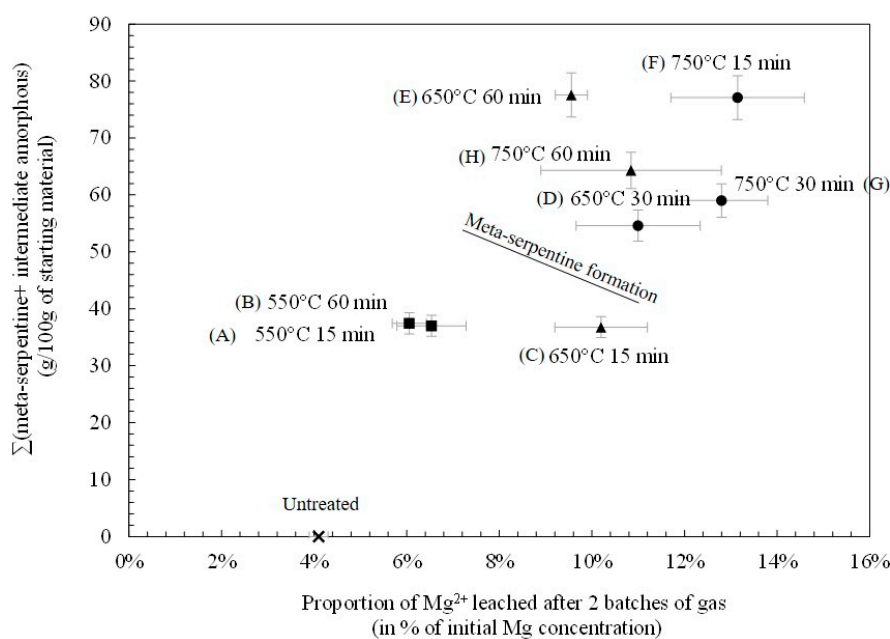


**Figure 3.** Extracted plotted against the quantity of amorphous phases, being the sum of the intermediate amorphous components and meta-serpentine. (Squares, triangle, and circles stands for test temperature of 550 °C, 650 °C, and 750 °C, respectively).

### 3.3.2. Successive Batches Dissolution

Thermal treatment conditions of samples D and F (650 °C for 30 min and 750 °C for 15 min) are chosen to be tested on successive batches as they respectively are the recommended conditions in literature [22] and the conditions giving the highest proportion of  $Mg^{2+}$  leached after two batches of gas in our conditions. Figure 4 shows the cumulative proportion of  $Mg^{2+}$  leached after twelve batches of gas. After two batches of gas, the proportion of  $Mg^{2+}$  leached demonstrates a significant discrepancy from the previous results and the present one. Indeed, the sample treated at 650 °C for 30 min shows a similar proportion of  $Mg^{2+}$  leached to the one treated at 750 °C for 15 min. After 4 batches, the sample treated at 750 °C for 15 min is catching up with a proportion of  $Mg^{2+}$  leached higher by 5 wt % compared to the other sample. At the end of the 12 batches, 44.6 wt % of  $Mg^{2+}$  has been leached from the sample treated at 750 °C for 15 min against 32.4 wt % for the one treated at 650 °C for 30 min. For the sample treated at 650 °C for 30 min, the proportions of  $Mg^{2+}$  leached reached a plateau close to 0.5 wt % during the tenth batch, suggesting that almost all of the  $Mg^{2+}$  available in the present dissolution conditions might have been leached. This occurred with at 750 °C after 15 min, which indicates that the plateau has not been reached yet, suggesting that more batches of  $CO_2$  could allow a higher proportion of  $Mg^{2+}$  leached. As the solution is refreshed for every two batches of gas, the limiting factor is the availability of the  $Mg^{2+}$  and not the saturation of the solution.

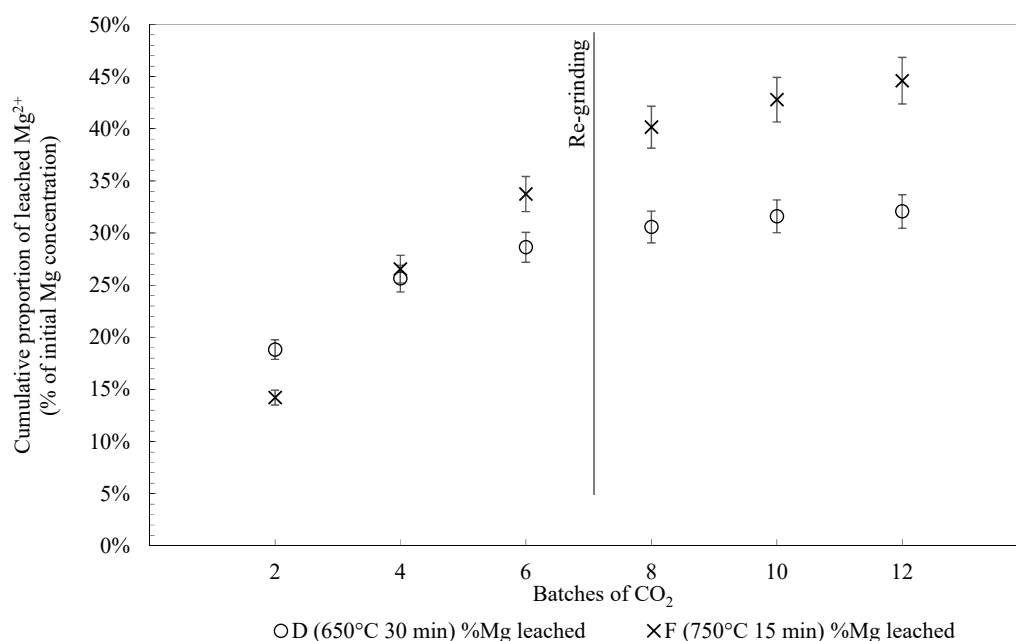


**Figure 4.** The  $Mg^{2+}$  leached (expressed in percent of initial  $Mg^{2+}$  concentration in the solid) for samples treated at 650 °C for 30 min (blue) and at 750 °C for 15 min (green).

The increase in the slope of the curves between the batches 6 and 8 demonstrate the slight effect of the grinding on the material after the batch 6. Pasquier et al. [30] demonstrated that the effect of the passivation silica layer, formed during dissolution, can be reduced by grinding and so revive the leaching of  $Mg^{2+}$ . Nevertheless, studies from the Carmex project [52,53]) show that a continuous mechanical exfoliation of the passivation layer as it forms on the grains would be a promising way to avoid the need for regrinding after six batches of gas.

### 3.4. Mineralogical Assemblage and Carbonation

As the hydroxyl groups escape the serpentine octahedral sheets, the remaining atoms of Mg and Si are reorganized through the amorphous components. As the temperature increases, serpentine is transformed into amorphous phases, then recrystallizes into forsterite.

The best mineralogical assemblage is shown to be a mixture of amorphous phases, as observed in sample F with the highest proportion of  $Mg^{2+}$  leached after both two batches and successive batches carbonation tests. McKelvy et al. [21] observed significantly higher carbonation reaction rates in the presence of amorphous meta-serpentine, formed above 610 °C, than in the presence of  $\alpha$ -meta-serpentine formed below 580 °C and identified as intermediate amorphous components here. When structurally stable Mg-bearing phases are present in the assemblage, such as serpentine or forsterite, material reactivity decreases. In serpentine, Mg atoms are bonded to the hydroxyls groups whereas in forsterite, they are ionically bonded to silica tetrahedron [54]. The differentiation of the two amorphous phases based on the proposed calculation in this paper were revealed to be accurate because the sample showing the highest value of metaserpentine appeared to be the one demonstrating the highest proportion of  $Mg^{2+}$  leached, in accordance with observations proposed in the literature.

Moreover, reactivity appears to be affected more by mineralogy than by surface area. Larachi et al. [15] provide surface area measurements on calcined samples, from 300 °C to 1200 °C, showing that it tends to decrease with increasing temperature as dehydroxylation occurs.

Furthermore, observations made here are in accordance to those made by other authors regarding the mineralogical transformations occurring during thermal activation and dehydroxylation [21,22]. Nevertheless, a shift of ideal temperature is observed, as observations made by others suggest that reactions at 650 °C were more likely to occur, rather than at 750 °C as occurred in the present study. Such

a change can be attributed to numerous factors such as the initial material mineralogy, the experimental set up, and the methodology used to evaluate activation efficiency. For instance, Li et al., [22] used hydrochloric acid to perform lixiviation tests, which is far from neutral pH and weak acid conditions used in the present study. On the other hand, McKelvy et al.'s [21] work set the basis of serpentine dehydroxylation understanding using TGA/DTA and XRD. Conversely, their carbonation conditions used high temperature and supercritical CO<sub>2</sub>, which is again far from the conditions tested here. Based on their results, past ideal activation conditions were shown to be effective, but not necessarily optimal. Therefore, the present results highlight the importance of considering the mineralogical assemblage alongside the thermal treatment parameters (temperature and residence time). Such an approach will allow us to take into account the effect of the initial material composition and potential specificity of the activation conditions/technique. Indeed, conditions in a rotary kiln will be very different from a furnace or a fluidized bed. As results, a study of the mineralogical assemblage can lead to an accurate optimization of heat activation operating conditions in accordance with the material activated and the equipment used.

#### 4. Conclusions

In this study, a novel approach of amorphous phase quantification, resulting from serpentine thermal activation, is introduced. It enables a better understanding of their implications in serpentine dissolution using carbonic acid as a lixiviant, in similar conditions to those used in the direct flue gas mineral carbonation process developed at INRS. The following conclusions can be made from this study:

- (i) It is possible to differentiate and quantify intermediate amorphous phases and metaserpentine formed during dehydroxylation of serpentine and correlate these values to the efficiency of carbonation reaction. In a static furnace, treatment at 750 °C for 15 min leads to the formation of 27.2 g/100 g of starting material of meta-serpentine.
- (ii) Thermally produced amorphous phases enhance Mg<sup>2+</sup> solubility during carbonation reaction. Furthermore, the formation of meta-serpentine, resulting in a complete dehydroxylation, significantly upgrades Mg<sup>2+</sup> leaching yield.
- (iii) The crystallization of forsterite decreases the sample dissolution potential by limiting the amount of Mg<sup>2+</sup> accessible for leaching in the present dissolution conditions.
- (iv) Adjusting thermal activations parameters (temperature and residence time) led to an increase of 39% of Mg<sup>2+</sup> leached during the carbonation reaction.

**Author Contributions:** Methodology, C.D.B., L.C.-P., G.D., J.-F.B., M.C.I., G.M.; formal analysis, C.D.B.; writing—original draft preparation, C.D.B., L.C.-P., G.D., J.-F.B., M.C.I. and G.M.; writing—review and editing, C.D.B., L.C.-P.; supervision, L.C.-P., G.D., J.-F.B., M.C.I. and G.M.; project administration, G.M.; funding acquisition, L.C.-P., G.D., J.-F.B., M.C.I. and G.M.

**Funding:** This research was funded by Fond de Recherche Quebecois en Nature et Technology, projet de recherche en équipe 2015–2016.

**Acknowledgments:** This research was funded by 'projet de recherche en équipe' grant from FRQNT. The authors would like to thank Matti Raudsepp, Kate Carroll, Ian Power from the University of British Columbia (Vancouver, Canada) and Connor Turvey from Monash University (Melbourne, Australia) for their advice and help on the XRD and Rietveld refinement application to the serpentine minerals.

**Conflicts of Interest:** The authors declare no conflict of interest.

#### References

1. IPCC. *Climate Change 2014: Synthesis Report. Contribution of Working Groups I, II and III to the Fifth Assessment Report of the Intergovernmental Panel on Climate Change*; Core Writing Team, Pachauri, R.K., Meyer, L.A., Eds.; IPCC: Geneva, Switzerland, 2014; p. 151.
2. Lackner, K.S.; Wendt, C.H.; Butt, D.P.; Joyce, B.L.; Sharp, D.H. Carbon dioxide disposal in carbonate minerals. *Energy* **1995**, *20*, 1153–1170. [[CrossRef](#)]

3. Seifritz, W. CO<sub>2</sub> disposal by means of silicates. *Nature* **1990**, *345*, 486. [CrossRef]
4. Maroto-Valer, M.M.; Fauth, D.J.; Kuchta, M.E.; Zhang, Y.; Andrésen, J.M. Activation of magnesium rich minerals as carbonation feedstock materials for CO<sub>2</sub> sequestration. *Fuel Process. Technol.* **2005**, *86*, 1627–1645. [CrossRef]
5. Hänchen, M.; Prigiobbe, V.; Baciocchi, R.; Mazzotti, M. Precipitation in the Mg-carbonate system: Effects of temperature and CO<sub>2</sub> pressure. *Chem. Eng. Sci.* **2008**, *63*, 1012–1028. [CrossRef]
6. Harrison, A.L.; Power, I.M.; Dipple, G.M. Accelerated carbonation of brucite in mine tailings for carbon sequestration. *Environ. Sci. Technol.* **2012**, *47*, 126–134. [CrossRef]
7. Page, N.J. Chemical differences among the serpentine polymorphs. *Am. Mineral.* **1968**, *53*, 201–215.
8. Goff, F.; Guthrie, G.D.; Lipin, B.; Fite, M.; Chipera, S.; Counce, D.A.; Kluk, E.; Ziock, H. *Evaluation of Ultramafic Deposits in the Eastern United States and Puerto Rico as Sources of Magnesium for Carbon Sequestration*; Los Alamos National Laboratory: Los Alamos, NM, USA, 2000; p. 30.
9. Nagamori, M.; Plumpton, A.J.; Le Houillier, R. Activation of magnesia in serpentine by calcination and the chemical utilization of asbestos tailings, A review. *C. Bull.* **1980**, *73*, 144–156.
10. Luce, R.W.; Bartlett, R.W.; Parks, G.A. Dissolution kinetics of magnesium silicates. *Geochim. Cosmochim. Acta* **1972**, *36*, 35–50. [CrossRef]
11. Stumm, W.; Morgan, J.J. *Aquatic Chemistry: An Introduction Emphasizing Chemical Equilibria in Natural Waters*; John Wiley and Sons: Hoboken, NJ, USA, 1981.
12. Aruja, E. An X-ray study of crystal-structure of antigorite. *Mineral. Mag.* **1994**, *27*, 11.
13. Nagy, B.; Faust, G. Serpentes: Natural mixtures of Chrysotile and antigorite. *Am. Mineral.* **1956**, *41*, 817–838.
14. Wicks, F.J.; Whittaker, E.J.W. Serpentine textures and serpentization. *Can. Mineral.* **1977**, *15*, 459–488.
15. Larachi, F.; Daldoul, I.; Beaudoin, G. Fixation of CO<sub>2</sub> by chrysotile in low-pressure dry and moist carbonation: Ex-situ and in-situ characterizations. *Geochim. Cosmochim. Acta* **2010**, *74*, 3051–3075. [CrossRef]
16. Mellini, M.; Zanazzi, P.F. Crystal structures of lizardite-1T and lizardite-2H1 from Coli, Italy. *Am. Mineral.* **1987**, *72*, 943–948.
17. Turci, F.; Tomatis, M.; Mantegna, S.; Cravotto, G.; Fubini, B. A new approach to the decontamination of asbestos-polluted waters by treatment with oxalic acid under power ultrasound. *Ultrason. Sonochem.* **2008**, *15*, 420–427. [CrossRef] [PubMed]
18. Ball, M.C.; Taylor, H.F.W. The dehydration of chrysotile in air and under hydrothermal conditions. *Mineral. Mag.* **1963**, *33*, 467–482. [CrossRef]
19. Brindley, G.W.; Hayami, R. Mechanism of formation of forsterite and enstatite from serpentine. *Mineral. Mag.* **1965**, *35*, 189–195. [CrossRef]
20. Brindley, G.W.; Hayami, R. Kinetics and mechanisms of dehydration and recrystallization of serpentine. *Clays Clay Miner.* **1965**, *12*, 35–37. [CrossRef]
21. McKelvy, M.J.; Chizmeshya, A.V.; Diefenbacher, J.; Béarat, H.; Wolf, G. Exploration of the role of heat activation in enhancing serpentine carbon sequestration reactions. *Environ. Sci. Technol.* **2004**, *38*, 6897–6903. [CrossRef]
22. Li, W.; Li, W.; Li, B.; Bai, Z. Electrolysis and heat pretreatment methods to promote CO<sub>2</sub> sequestration by mineral carbonation. *Chem. Eng. Res. Des.* **2009**, *87*, 210–215. [CrossRef]
23. Farhang, F.; Rayson, M.; Brent, G.; Hodgins, T.; Stockenhuber, M.; Kennedy, E. Insights into the dissolution kinetics of thermally activated serpentine for CO<sub>2</sub> sequestration. *Chem. Eng. J.* **2017**, *330*, 1174–1186. [CrossRef]
24. Gerdemann, S.J.; O'Connor, W.K.; Dahlin, D.C.; Penner, L.R.; Rush, H. Ex situ aqueous mineral carbonation. *Environ. Sci. Technol.* **2007**, *41*, 2587–2593. [CrossRef] [PubMed]
25. O'Connor, W.K.; Dahlin, D.C.; Rush, G.E.; Gerdemann, S.J.; Penner, L.R.; Nilsen, D.N. Aqueous Mineral Carbonation; Final Report DOE/ARC-TR-04-002. 2005, p. 462. Available online: [https://www.researchgate.net/profile/William\\_Oconnor8/publication/315844800\\_Aqueous\\_Mineral\\_Carbonation\\_Mineral\\_Availability\\_Pretreatment\\_Reaction\\_Parametrics\\_and\\_Process\\_Studies/links/58ebb247a6fdcc965767765f/Aqueous-Mineral-Carbonation-Mineral-Availability-Pretreatment-Reaction-Parametrics-and-Process-Studies.pdf](https://www.researchgate.net/profile/William_Oconnor8/publication/315844800_Aqueous_Mineral_Carbonation_Mineral_Availability_Pretreatment_Reaction_Parametrics_and_Process_Studies/links/58ebb247a6fdcc965767765f/Aqueous-Mineral-Carbonation-Mineral-Availability-Pretreatment-Reaction-Parametrics-and-Process-Studies.pdf) (accessed on 3 November 2019).

26. Gerdemann, S.J.; Dahlin, D.C.; O'Connor, W.K.; Penner, L.R. Carbon dioxide sequestration by aqueous mineral carbonation of magnesium silicate minerals. In *Greenhouse gas Technologies*; Albany Research Center (ARC): Albany, OR, USA, 2003; p. 8.
27. Mann, J. Serpentine Activation for CO<sub>2</sub> Sequestration. Ph.D. Thesis, University of Sydney, Sydney, Australia, 2014; p. 274.
28. Sanna, A.; Wang, X.; Lacinska, A.; Styles, M.; Paulson, T.; Maroto-Valer, M.M. Enhancing Mg extraction from lizardite-rich serpentine for CO<sub>2</sub> mineral sequestration. *Miner. Eng.* **2013**, *49*, 135–144. [[CrossRef](#)]
29. Mercier, G.; Blais, J.-F.; Cecchi, E.; Veetil, S.P.; Pasquier, L.-C.; Kentish, S. Carbon Dioxide Chemical Sequestration from Industrial Emissions by Carbonation. U.S. Patent 9.440,189 B2, 13 September 2016.
30. Pasquier, L.-C.; Mercier, G.; Blais, J.F.; Cecchi, E.; Kentish, S. Reaction mechanism for the aqueous-phase mineral carbonation of heat-activated serpentine at low temperatures and pressures in flue gas conditions. *Environ. Sci. Technol.* **2014**, *48*, 5163–5170. [[CrossRef](#)] [[PubMed](#)]
31. Pasquier, L.-C.; Mercier, G.; Blais, J.F.; Cecchi, E.; Kentish, S. Parameters optimization for direct flue gas CO<sub>2</sub> capture and sequestration by aqueous mineral carbonation using activated serpentinite based mining residues. *Appl. Geochem.* **2014**, *50*, 66–73. [[CrossRef](#)]
32. Moreno Correia, M.J. Optimisation de la Précipitation des Carbonates de Magnésium pour L'application dans un Procédé de Séquestration de CO<sub>2</sub> par Carbonatation Minérale de la Serpentine. Master's Thesis, Université du Québec, Québec, QC, Canada, 2018; p. 125.
33. Pasquier, L.-C.; Mercier, G.; Blais, J.-F.; Cecchi, E.; Kentish, S. Technical and economic evaluation of a mineral carbonation process using southern Québec mining wastes for CO<sub>2</sub> sequestration of raw flue gas with by-product recovery. *Int. J. Greenh. Gas Control* **2016**, *50*, 147–157. [[CrossRef](#)]
34. Kemache, N.; Pasquier, L.-C.; Cecchi, E.; Mouedhen, I.; Blais, J.-F.; Mercier, G. Aqueous mineral carbonation for CO<sub>2</sub> sequestration: From laboratory to pilot scale. *Fuel Process. Technol.* **2017**, *166*, 209–216. [[CrossRef](#)]
35. Kemache, N.; Pasquier, L.-C.; Mouedhen, I.; Cecchi, E.; Blais, J.-F.; Mercier, G. Aqueous mineral carbonation of serpentinite on a pilot scale: The effect of liquid recirculation on CO<sub>2</sub> sequestration and carbonate precipitation. *Appl. Geochem.* **2016**, *67*, 21–29. [[CrossRef](#)]
36. Aumento, F. *Serpentine Mineralogy of Ultrabasic Intrusion in Canada and on the Mid-Atlantic Ridge*; Department of Energy, Mines and Resources: Ottawa, ON, Canada, 1970.
37. Tertian, R.; Claisse, F. *Principles of Quantitative X-ray Fluorescence Analysis*; Wiley-Heyden: London, UK, 1982.
38. Wilson, S.A.; Raudsepp, M.; Dipple, G.M. Verifying and quantifying carbon fixation in minerals from serpentine-rich mine tailings using the Rietveld method with X-ray powder diffraction data. *Am. Mineral.* **2006**, *91*, 1331–1341. [[CrossRef](#)]
39. Bish, D.L.; Howard, S. Quantitative phase analysis using the Rietveld method. *J. Appl. Crystallogr.* **1988**, *21*, 86–91. [[CrossRef](#)]
40. Pawley, G.S. Unit-Cell Refinement from Powder Diffraction scans. *J. Appl. Crystallogr.* **1981**, *14*, 357–361. [[CrossRef](#)]
41. Raudsepp, M.; Pani, E.; Dipple, G. Measuring mineral abundance in skarn; I, The Rietveld method using X-ray powder-diffraction data. *Can. Mineral.* **1999**, *37*, 1–15.
42. Rietveld, H.M. A Profile Refinement Method for Nuclear and Magnetic Structures. *J. Appl. Crystallogr.* **1969**, *2*, 65–71. [[CrossRef](#)]
43. Turvey, C.C.; Wilson, S.A.; Hamilton, J.L.; Southam, G. Field-based accounting of CO<sub>2</sub> sequestration in ultramafic mine wastes using portable X-ray diffraction. *Am. Mineral.* **2017**, *102*, 1302–1310. [[CrossRef](#)]
44. Scarlett, N.V.Y.; Madsen, I.C. Quantification of phases with partial or no known crystal structures. *Powder Diffr.* **2006**, *21*, 278–284. [[CrossRef](#)]
45. Le Bail, A. Whole powder pattern decomposition methods and applications: A retrospection. *Powder Diffr.* **2005**, *20*, 316–326. [[CrossRef](#)]
46. Falini, G.; Foresti, E.; Gazzano, M.; Gualtieri, A.F.; Leoni, M.; Lesci, I.G.; Roveri, N. Tubular-Shaped Stoichiometric Chrysotile Nanocrystals. *Chem. A Eur. J.* **2004**, *10*, 3043–3049. [[CrossRef](#)]
47. Du Breuil, C.; Pasquier, L.C.; Dipple, G.; Blais, J.F.; Iliuta, M.C.; Mercier, G. Impact of particle size in serpentine thermal treatment: Implications for serpentine dissolution in aqueous-phase using CO<sub>2</sub> in flue gas conditions. *Appl. Clay Sci.* **2019**, *182*, 105286. [[CrossRef](#)]
48. Jolicoeur, C.; Duchenes, D. Infrared and thermogravimetric studies of the thermal degradation of chrysotile asbestos fibers: Evidence for matrix effects. *Can. J. Chem.* **1981**, *59*, 1521–1526. [[CrossRef](#)]

49. Viti, C. Serpentine minerals discrimination by thermal analysis. *Am. Mineral.* **2010**, *95*, 631–638. [[CrossRef](#)]
50. Balucan, R.D.; Dlugogorski, B.Z. Thermal activation of antigorite for mineralization of CO<sub>2</sub>. *Environ. Sci. Technol.* **2013**, *47*, 182–190. [[CrossRef](#)]
51. Hora, Z. Ultramafic hosted chrysotile asbestos. In *Fieldwork*; British Columbia Geological Survey: Victoria, BC, Canada, 1997; p. 4.
52. Bodéan, F.; Bourgeois, F.; Petiot, C.; Augé, T.; Bonfils, B.; Julcour-Lebigue, C.; Guyot, F.; Boukary, A.; Tremosa, J.; Lassin, A.; et al. Ex situ mineral carbonation for CO<sub>2</sub> mitigation: Evaluation of mining waste resources, aqueous carbonation processability and life cycle assessment (Carmex project). *Miner. Eng.* **2014**, *59*, 52–63. [[CrossRef](#)]
53. Julcour, C.; Bourgeois, F.; Bonfils, B.; Benhamed, I.; Guyot, F.; Bodéan, F.; Petiot, C.; Gaucher, É.C. Development of an attrition-leaching hybrid process for direct aqueous mineral carbonation. *Chem. Eng. J.* **2015**, *262*, 716–726. [[CrossRef](#)]
54. Birle, J.; Gibbs, G.; Moore, P.; Smith, J. Crystal structures of natural olivines. *Am. Mineral.* **1968**, *53*, 807.



© 2019 by the authors. Licensee MDPI, Basel, Switzerland. This article is an open access article distributed under the terms and conditions of the Creative Commons Attribution (CC BY) license (<http://creativecommons.org/licenses/by/4.0/>).